Subaqueous barchan dunes in turbulent shear flow. Part 1: Dune motion

By E. M. FRANKLIN AND F. CHARRU

Institut de Mécanique des Fluides de Toulouse - CNRS–Université de Toulouse - Allée C. Soula, 31400 Toulouse, France.

(Received ?? and in revised form ??)

Experiments are reported on the formation and migration of isolated dunes in a turbulent channel flow. These dunes have a very robust crescentic shape with horns pointing downstream, very similar to that of the barchan dunes observed in deserts at a much larger scale. Their main geometrical and dynamical properties are studied in detail, for four types of grains: the conditions for their formation, their morphology, the threshold shear stress for their motion, their velocity, erosion rate, minimum size, and the longitudinal stripes of grains hollowed by fluid streaks in the boundary layer. In particular, the law for the dune velocity is found to involve two dimensionless parameters, the Shields number and the sedimentation Reynolds number, in contrast with predictions based on classical laws for particle transport. As the dune migrates, its size slowly decreases because of a small leakage of particles at the horn tips, and the erosion law is given. A minimum size is evidenced, which is shown to increase with the friction velocity and scale with a settling length.

1. Introduction

When sand grains are entrained by an air flow over a non-erodible ground, or with limited sediment supply from the bed, they form dunes showing a remarkable crescentic shape with horns pointing downstream. These dunes, known as barchan dunes, are commonly observed in deserts, with height of a few meters and velocity of a few tens of meters per year. In his famous book, Bagnold (1941) first pointed out their significance for understanding the physics of blown sand. Their outstanding shape and stability properties have triggered a number of studies, aiming at understanding the conditions for their formation, their migration velocity and time evolution, and also the striking existence of a minimum length, of about ten meters, below which no dune is observed. A model accounting for their main properties was derived by Kroy, Sauermann & Hermann (2002) and Andreotti, Claudin & Douady (2002a, 2002b), from calculations of the shear stress at the dune surface by Hunt, Leibovich & Richards (1988) and a relaxation equation for the sand flux accounting for the retarding effect of grain inertia (Sauermann, Kroy & Hermann 2001).

Similar barchan dunes have also been observed under water flows, with, however, much shorter lengths than in air, when, again, the sediment supply is limited. Such dunes formed in an open channel flow are reported by Mantz (1978), with typical width of about three centimeters (Figure 1a); in this paper the resemblance with the aeolian dunes observed by Bagnold was noted. This resemblance was investigated further by Hersen, Douady & Andreotti (2002) and Hersen (2005) from experiments in which the dunes were formed on a tray oscillating asymmetrically in a water tank. Barchan dunes

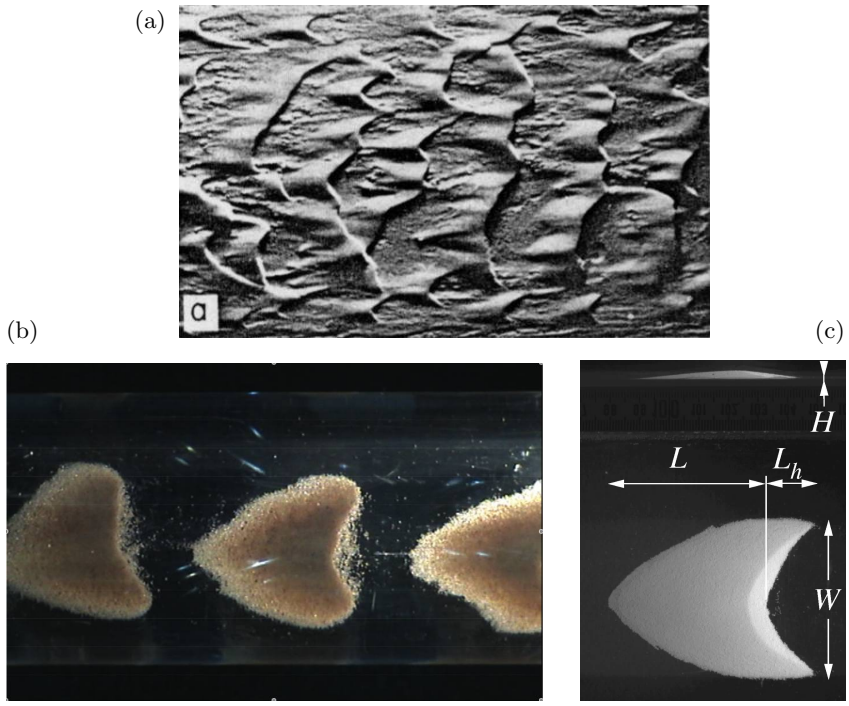

FIGURE 1. Subaqueous barchan dunes. (a), in an open channel (Mantz 1978); (b) in a pipe (Al-lababidi *et al.* 2008); (c), in a closed channel from the present experiments, top and side views, and definition of the characteristic lengths (zircone beads with diameter $d = 0.2$ mm, dune length $L = 50$ mm). Water flows from left to right.

formed in a circular pipe are also clearly visible in a photograph shown by Al-lababidi *et al.* (2008) (Figure 1b); although this paper does not comment on their particular shape, it discusses the increase of the pressure drop and potential damages that isolated dunes may cause in industrial pipe flows.

Barchan dunes under water have received much less attention than aeolian dunes, and important issues related to their dynamics remain unanswered. These issues are (i) the conditions under which barchan dunes form and disappear, and their migration velocity; (ii) the distributions of fluid velocity and shear stress over the dune surface, and the resulting particle flux; (iii) their stability properties and interactions in a field: splitting and merging of dunes of different size and velocity, existence of an eventual stable equilibrium size. This paper aims at answering these questions, from experiments in a turbulent channel flow. The present Part One is devoted to the first issue of the formation and velocity of dunes; the following Part Two will deal with the second issue of the fluid motion near the dune. In this Part One, the experimental set-up and turbulent water flow are described in §2. The formation, morphology and migration velocity of the barchan dunes are analysed in §3. The results are summarized and discussed in §4.

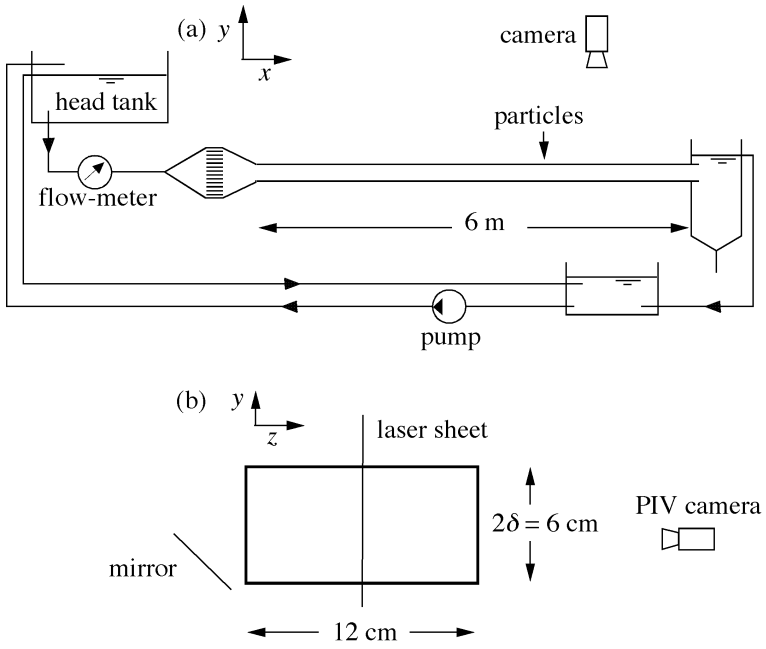

FIGURE 2. Sketch of the experimental arrangement. (a), side-view; (b), cross-section of the channel.

2. Experimental arrangement and channel flow

2.1. *Experimental arrangement*

The experimental arrangement mainly consists of a horizontal plexiglass channel, six meters long, with rectangular cross-section of height $2\delta = 60$ mm and width $b = 120$ mm (Figure 2a). Water flows from a head-tank with free surface 2.5 meters above the channel, and enters the channel through a divergent-convergent device with a honeycomb section in order to suppress large eddies and homogeneize the small-scale turbulence. At the open end of the channel, particles are separated by sedimentation in a large tank, and a pump drives the water up to the head-tank. The volumetric flow rate is measured with an electromagnetic flow-meter.

The particles were deposited in the channel, previously filled with water, with the help of a syringe through a small hole in the upper wall located at 4.15 m form the entrance. The sand settled in the water at rest and formed a conical heap. Then the flow was started up, and the heap deformed into a barchan dune. The evolution of the shape of the dune was recorded with a video camera placed above the channel and mounted on a travelling system. The resolution of the camera was 2048×2048 pixels, with field of view at the bottom wall of about 140×140 mm^2. The side view of the dune was recorded on the same images thanks to a mirror inclined at 45°, as shown in Figure 2b. A sample of the resulting image is shown in Figure 1c.

Fluid velocity measurements were performed in the vertical mid-plane of the channel using Particle Image Velocimetry (PIV), as sketched in Figure 2b. A vertical laser sheet of thickness of 1 mm was generated by a 30mJ Nd:Yag double-pulse laser, and illuminated fluorescent rhodamine encapsulated in small acrylic beads, of density $1110\,\mathrm{kg\,m^{-3}}$ and diameter of about 10 μm. A 1280×1024 px 12-bit CCD camera was used to capture the images, with a 50 mm or 60 mm Nikon lens. The time interval between the two images of a pair was in the range 224–848 μs, and the sampling frequency of the pairs

were in the range 1–4 Hz. A high-pass filter interposed between the laser sheet and the camera allowed suppression of the light scattered by the dunes and channel walls. For flow measurements over the whole channel height, the field of view was 85×68 mm^2, whereas for closer inspection near the dune, a smaller field of view was used, of 22×17 mm^2. The PIV images were processed with the software PIVIS developed at IMFT, with correlation boxes of 16×16 pixels with sub-pixel accuracy; the resulting spatial resolution of the velocity field was 1 mm with the large field, and 0.15 mm with the small one (in the latter case an overlap of 50% of the correlation boxes was used). Convergence of the time-averaged longitudinal and vertical velocities, U and V, was achieved within 1% with about 30 frames, whereas a larger number, of about 200, was required for the Reynolds stresses $\overline{u'^2}$, $\overline{v'^2}$ and $\overline{u'v'}$.

2.2. *Channel flow*

The flow velocity $\langle U \rangle$, defined as the ratio of the measured volumetric flow rate and the channel cross-section, was varied between 0.15 and 0.4 m s^{-1}. The corresponding Reynolds number

$$Re = \frac{\langle U \rangle 2\delta}{\nu} \tag{2.1}$$

was in the range $9000 - 24000$, so that the flow was turbulent.

Figure 3a displays mean velocity profiles $U(y)$ in the mid-plane, four meters downstream of the inlet, for six Reynolds numbers in the range 14000–21000. The profiles appear to be symmetric with respect to the horizontal mid-plane, as expected. The depth-averaged velocity is slightly larger than the flow velocity $\langle U \rangle$, by about 4%, which difference corresponds to the retarding effect of the lateral walls. Plotting these velocities with semi-logarithmic scales (not shown) reveals log-regions spanning approximately from 2 to 10 mm from the walls, allowing the friction velocity u_* to be determined by linear regression with $\kappa = 0.41$ for the Kármán coefficient. Figure 3b displays the velocity profiles in the lower half of the channel in wall units, $U^+ = U/u_*$ versus $y^+ = yu_*/\nu$, for six Reynolds numbers. It appears that for y^+ in the range 30–200, data points collapse onto the same curve

$$U^+ = \frac{1}{\kappa} \ln y^+ + B, \tag{2.2}$$

with the coefficients $\kappa = 0.41$ and $B = 5.5$ having their usual values (Davidson 2004). Note that these coefficients have been shown to decrease slightly with Reynolds number and reach constant values for large Reynolds number only (Nagib & Chauhan 2008); these small variations have not been taken into account here. A slow secondary flow normal to the main flow is known to develop in rectangular ducts, with typical velocity of about 1% of the mean longitudinal velocity (Melling & Whitelaw 1976). This secondary flow is expected to have negligible effect on the motion of dunes, and has not been measured.

Figure 4 shows the variation of the friction coefficient $c_f = u_*^2/\frac{1}{2}\langle U \rangle^2$ with Reynolds number, together with the Blasius correlation

$$c_f = 0.079\,(1.33\,Re)^{-1/4}. \tag{2.3}$$

In this equation, the factor 1.33 arises because the Reynolds number involved in the Blasius correlation is based on the hydraulic diameter, and the friction velocity represents the average over the perimeter of the channel (Schlichting 1979). It appears from Figure 4 that the Blasius correlation provides a good fit of the measured friction velocities.

Figure 5a displays profiles of the Reynolds stress $-\overline{u'v'}$, normalized by u_*^2. This stress is antisymmetric and varies linearly in the middle of the channel, as expected in a pressure-driven channel flow. Its maximum is slightly lower than u_*^2 and located at $y/\delta \approx 0.2$; closer

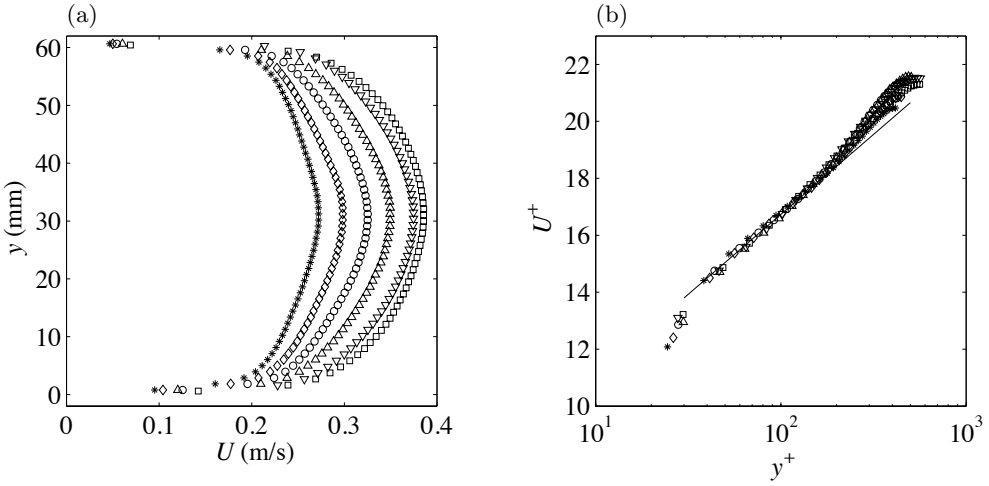

FIGURE 3. Velocity profiles $U(y)$ in the vertical mid-plane of the channel for $Re = 13900$ ($*$), 15000 ($\diamond$), 16200 ($\circ$), 17400 ($\triangle$), 18500 ($\triangledown$) and 19700 ($\square$); (a), in linear dimensional scales; (b) in semilog wall scales in the lower half of the channel, with the straight line corresponding to equation (2.2).

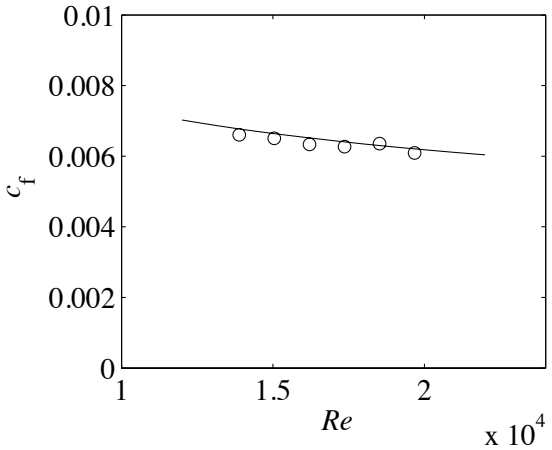

FIGURE 4. ($\circ$), Friction coefficient versus Reynolds number; (—), Blasius correlation (2.3).

to the walls where viscous effects are no longer negligible, it decreases to zero. Figure 5b displays the same profiles in wall units, magnifying the region close to the maximum; this plot confirms that stresses are nearly uniform in the region $30 < y^+ < 200$ where the log-law holds.

The Reynolds stresses $\overline{u'^2}$ and $\overline{v'^2}$, not shown, have also been determined and their profiles agree with those shown in the literature (Davidson 2004). In particular, $\overline{u'^2}$ is minimum and about u_*^2 at mid-height ($y/\delta = 1$), it increases towards the walls and reaches a maximum of about 4–5 u_*^2 in the log-region; similarly, $\overline{v'^2}$ is minimum and

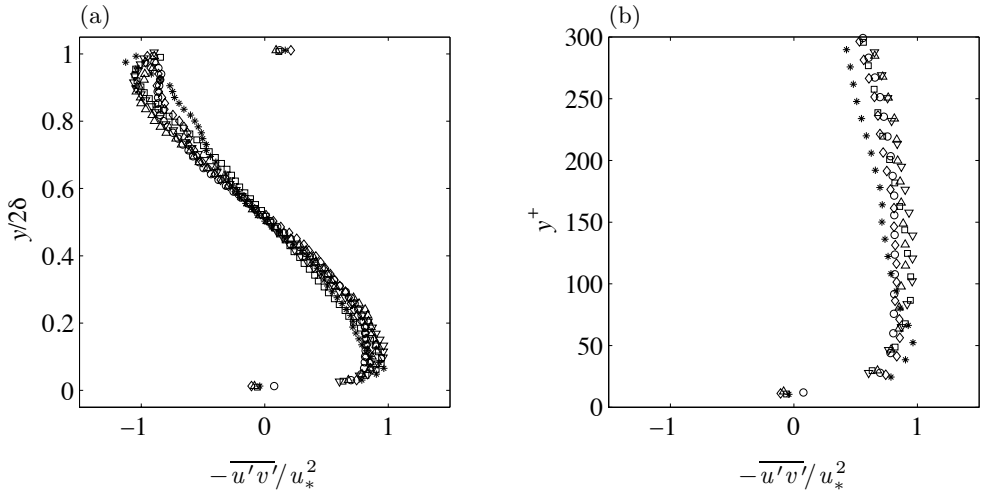

FIGURE 5. Vertical profiles of the normalized Reynolds stresses $-\overline{u'v'}/u_*^2$ for the same Reynolds numbers as in Figure 3 ; (a), over the whole channel height; (b), close to the bottom wall in wall units. Symbols: same as in Figure 3.

about $0.5\,u_*^2$ at mid-height, it increases towards the walls and reaches a maximum about u_*^2 in the log-region ($y^+ \approx 100$).

From the above discussion, it can be concluded that in the last third of the channel where the dune motion was observed, the water flow has the classical features of a fully-developed turbulent channel flow. In particular, near the lower wall and up to a height of about one centimeter, the mean velocity profile is logarithmic with friction velocity u_* given by the Blasius correlation (2.3); in this region, the Reynolds stress $-\overline{u'v'}$ is nearly uniform and close to u_*^2, as in a turbulent boundary layer with negligible pressure-gradient effect.

2.3. *Particles*

Four types of particles were used, whose properties are given in Table 1: series 1, 2 and 3 correspond to glass particles of median diameter $d = 0.12$, 0.20 and 0.51 mm, and series 4 to heavier zirconium particles† of diameter 0.19 mm. The standard deviation of the diameter distribution was about $0.2\,d$. The falling velocity $V_{\rm fall}$ shown in the table was obtained from the classical Schiller-Neuman correlation for the drag coefficient (Clift, Grace & Weber 1978), $C_D = 24/Re_{\rm fall}(1 + 0.15Re_{\rm fall}^{0.687})$ where the settling Reynolds number is defined as

$$Re_{\rm fall} = \frac{V_{\rm fall} d}{\nu}. \tag{2.4}$$

We finally define the particle Reynolds number and Shields number as

$$Re_p = \frac{u_{*d} d}{\nu}, \qquad \theta = \frac{\rho u_{*d}^2}{(\rho_p - \rho) g d} = \frac{u_{*d}^2}{V_{\rm ref}^2} \tag{2.5}$$

where $u_{*d} = 1.2\,u_*$ is a characteristic friction velocity on the dune (larger than the friction velocity u_* on the smooth wall, as explained in the following Section) and $V_{\rm ref} = ((\rho_p/\rho - 1)gd)^{1/2}$ is a reference settling velocity. Table 1 displays the maximum value

† The glass and zirconium particles were obtained from Sigmund Lindner GmbH, D-95485 Warmensteinach.

Series	d mm	ρ_p kg m^{-3}	$V_{\rm fall}$ mm s^{-1}	$Re_{\rm fall}$	$Re_{p,\max}$	$\theta_{\max}$	Symbol
1	0.12	2600	10.7	1.28	3.0	0.34	◇
2	0.18	2600	20.6	3.71	4.5	0.23	○
3	0.51	2600	78.4	40.0	12.9	0.08	□
4	0.19	3760	35.0	6.65	4.8	0.12	∗

TABLE 1. Particles properties, settling velocity $V_{\rm fall}$ and Reynolds number $Re_{\rm fall}$, maximum values of the particle Reynolds number Re_p and Shields number θ, and corresponding symbols in the figures.

of these numbers. Note that the particle Reynolds numbers was smaller than 13 for all experiments, so that small viscous effects on the grain motion are likely to be expected.

3. Dune motion

3.1. *Dune formation*

Once a conical heap of particles is formed in the channel as explained in the previous section, the flow is started up at a constant rate. The heap then deforms as shown in Figure 6, which displays the top view and side view (in the upper part of the photos, as given by the inclined mirror) of a typical heap, at six successive times. Due to strong erosion on the upstream face, the heap flattens, as it can be seen on the side views, and its horizontal area increases. A slip face develops on the lee-side where particles avalanche (the clearer region on the top views), and horns grow on both sides. On the fifth photograph ($t = 36$ s), the heap has reached a crescent-like shape typical of a barchan dune. The dune then propagates downstream, keeping the same shape. The equilibrium shape is reached as the displacement of the dune from its initial position is of the order of its length. Varying the shape of the initial heap does not change the final dune shape.

The dune propagates as the result of the erosion of a thin layer of particles at the surface of the upstream face; there, particles roll on each other, as over a flat bed (Mouilleron, Charru & Eiff 2009; Lajeunesse, Malverti & Charru 2010); contrary to what happens in air, no large saltating jumps were observed. As the particles reach the brink, they avalanche on the downstream face where the fluid shear stress nearly vanishes. Among the particles that arrive at the horn tips, most of them are driven towards the base of the slip face by the recirculating flow in the dune wake. However, a few of them are entrained downstream and leave the dune, so that the dune size slowly decreases with time.

As the dune propagates, one horn may become longer than the other, as shown in Figure 7; the longer horn generally looses more particles, so that its length decreases and the initial symmetry is recovered. However, when the dune approaches one of the side walls of the channel, the asymmetry may amplify: the longer horn eventually separates from the main dune and form a smaller dune propagating faster. Similar observations were made by Hersen (2005) for dunes over a tray undergoing asymmetric oscillations in a tank.

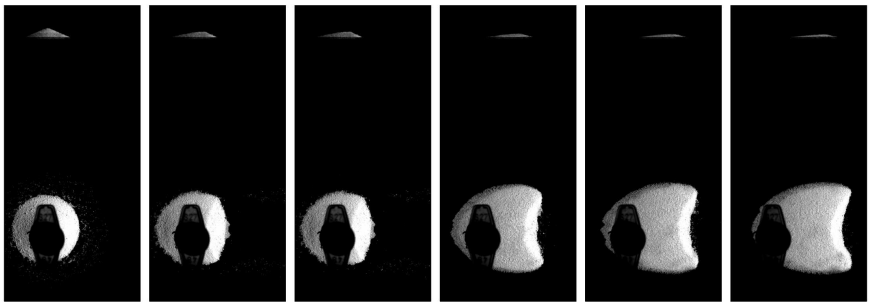

FIGURE 6. Side views (upper part of the pictures) and top views (lower part) of an initially conical heap of diameter 20 mm deposited from a syringe (the fixed black spot) and deformed by the water flow, at times $t = 0$, 9, 18, 27, 36 and 45 seconds. The flow, with $Re = 22200$, is from left to right.

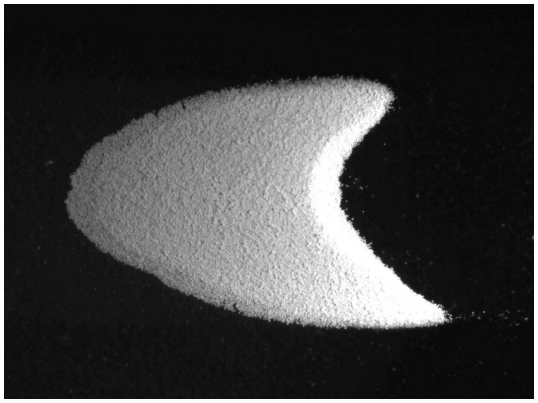

FIGURE 7. Top view of an asymmetric dune with different horn lengths; the dune width is $W = 5$ cm and the distance to the lateral walls of both horns is the same; the particles leaving the longer horn are clearly visible.

3.2. *Threshold shear stress for dune motion*

Since the initial heap is formed by sedimentation, the arrangment of the particles is loose and particles are easily moved by a small water flow. As the heap deforms, the packing density increases and particles move less easily (which phenomenon is known as armouring). Once the equilibrium shape is reached, a minimum water flow rate is then needed for moving the barchan dune. The criterion chosen for this minimum flow rate, not so easy to assess, was that a continuous motion over the dune surface must be visible. This criterion gave threshold conditions close to those obtained by extrapolating the dune velocity down to zero, see §3.4. Table 2 gives, for the four series of particles, the friction velocity u_* on the smooth wall corresponding to the threshold conditions, deduced from the Blasius correlation (2.3) (for the threshold experiments, particles have been re-sieved so that the diameters appearing in Table 2 are slightly different than those in Table 1).

The actual shear stress on the dune crest, say ρu_{*d}^2, is expected to be larger than

Series	d mm	D –	θ_t –	u_{*t} mm s^{-1}	u_* mm s^{-1}	u_{*t}/u_* –
1	0.11	2.75	0.073	11.2	9.0	1.24
2	0.21	5.26	0.047	12.4	10.7	1.16
3	0.53	13.3	0.031	15.9	13.1	1.22
4	0.21	6.31	0.042	15.4	11.9	1.29

TABLE 2. For each of the four series, dimensionless number D, corresponding threshold Shields number θ_t and threshold friction velocity u_{*t}, friction velocity at the onset of dune motion u_* as given by (2.3), and ratio u_{*t}/u_*.

that on the smooth wall, ρu_*^2, due to both form and roughness effects. This shear stress was estimated as follows. The threshold shear stress for particle motion on a flat bed corresponds a critical Shields number

$$\theta_t = \frac{\rho u_{*t}^2}{(\rho_p - \rho)gd}. \tag{3.1}$$

This number is about 0.05, and weakly depends on the particle Reynolds number (or the dimensionless number $D^3 = (\rho_p/\rho - 1)gd^3/\nu^2$ which represents a Reynolds number based on the Stokes falling velocity). For each series of particles, this number can be calculated using the empirical correlation $\theta_t(D)$ proposed by Soulsby & Whitehouse (1997). Then the corresponding threshold friction velocity on the dune, u_{*t}, can be obtained from (3.1). The friction velocity thus determined, as well as the ratio u_{*t}/u_*, are reported in Table 2. It appears that u_{*t}/u_* is approximately constant and close to 1.2. In other words, the actual shear stress on a dune is approximately $(1.2)^2 \approx 1.4$ times larger than that on the smooth wall, at the threshold conditions. Although this number might depend on the dune height, no significant variation was found, which is consistent with the fact that this height, in the range 1–7 mm, was much smaller than the channel height. More generally, for dune widths less than one-half of the channel width and dune heights less than one tenth of the channel height, confinement had negligible effect on the observations reported in this paper. A detailed analysis of the variation of the shear stress along the dune will be addressed in the second part of this paper.

3.3. *Dune morphology*

Since Bagnold's observations, the shape of aeolian barchan dunes, in particular their apparent scale invariance and the existence of a minimum size, has been extensively investigated (Sauerman *et al.* 2000; Andreotti, Claudin & Douady 2002a; Elbelrhiti, Andreotti & Claudin 2008). The length L, width W, height H and horn length L_h, as defined in Figure 1c, are the parameters generally reported. Measurements exhibit large scatter due to wind variations, but linear relationships emerge after averaging between the characteristic lengths, of the form $H = c_H(L - L_0)$. Typically, $c_H \approx 0.2$ and $L_0 \approx 10$ m; however, these coefficients depend on the dune field investigated. It has been noted that the offset length L_0 breaks the proportionality of the height and length, i.e. aeolian dunes are not scale invariant. The significance of this offset length has been related to the observation that all aeolian dunes are larger than a minimum size; this point will be discussed further in Section 3.6. Another point of the discussion is the position of the

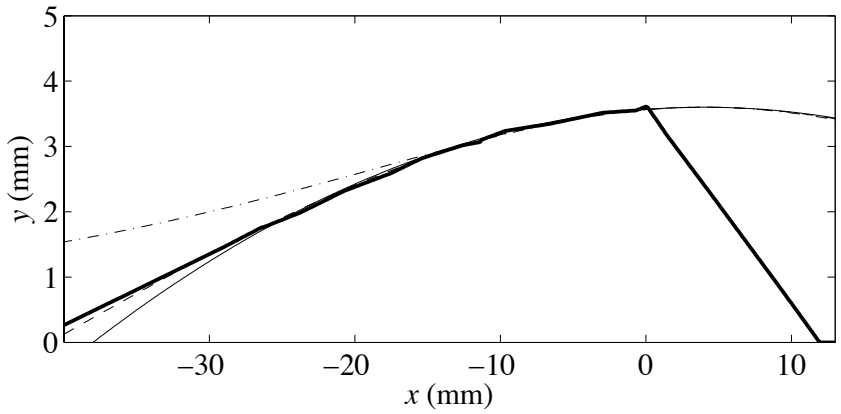

FIGURE 8. Typical profile of a dune. Thick line: measured profile; $(- \cdot -)$, fit (3.2) with $L = 38\,\mathrm{mm}$, $h_M = 3.6\,\mathrm{mm}$, and $x_M = 4\,\mathrm{mm}$; $(- -)$, fit from (3.3) with $L = 45\,\mathrm{mm}$ and the same h_M and x_M; (—) parabolic fit with $L = 42\,\mathrm{mm}$, and the same h_M and x_M.

dune top, which may coincide with the brink of the slip face for small dunes, or, for larger ones, correspond to the crest of a smooth dome located upstream of the brink.

As mentioned in the introduction, barchan dunes under water have already been reported, but with a centimetric size, much smaller than that of aeolian dunes. (The large dunes observed at the bottom of shallow seas or rivers, of a few meters high, are rather two-dimensional structures which have grown on erodible beds (ASCE 2002).) However, the question of their morphology and scale invariance has not been investigated yet.

The first point to address is the longitudinal profile $h(x)$ in the vertical symmetry plane of the dune, which is closely related to the particle flux as it will be shown in Section 3.4. Figure 8 displays the profile of a typical dune. The left side corresponds to the upstream face, with slope of the order of 7°, whereas the steeper right side corresponds to the horn; the avalanche face, hidden by the horn, has a slope close to 30°. The origin $x = 0$ corresponds to the highest point of the profile, which coincides with the position of the brink in the symmetry plane of the dune. The profile of a dune or hill often considered in theoretical analyses is the symmetrical bell shape (Benjamin 1959, Hunt, Leibovich & Richards 1988)

$$h(x) = \frac{h_M}{1 + (x - x_M)^2/L^2}. \tag{3.2}$$

Fitting the measured profile with this bell shape (the dotted-dashed line in the figure) shows that (i), eq. (3.2) represents nicely the upstream face near the brink ($-20 < x\,(\mathrm{mm}) < 0$) but decreases too slowly near the foot ($-40 < x\,(\mathrm{mm}) < -20$), and (ii), the top of the bell does not coincide with the brink, it is located downstream at a distance $x_M = 4\,\mathrm{mm} \approx h_M$. The parabolic shape suggested by Sauermann *et al.* (2000), $h(x) = h_M\,(1 - (x - x_M)^2/L^2)$, provides better agreement (plain line). The best fit over the whole profile was however provided by the cosine shape

$$h(x) = h_M\,\cos\frac{\pi(x - x_M)}{2L}, \tag{3.3}$$

with the same x_M and h_M (dashed line). The length $L = 45\,\mathrm{mm}$ for the cosine shape is slightly larger than for the bell and parabolic shapes, and close to the length $L = 48\,\mathrm{mm}$ defined in Figure 1c from the top view. The feature that the slope of the profile is positive

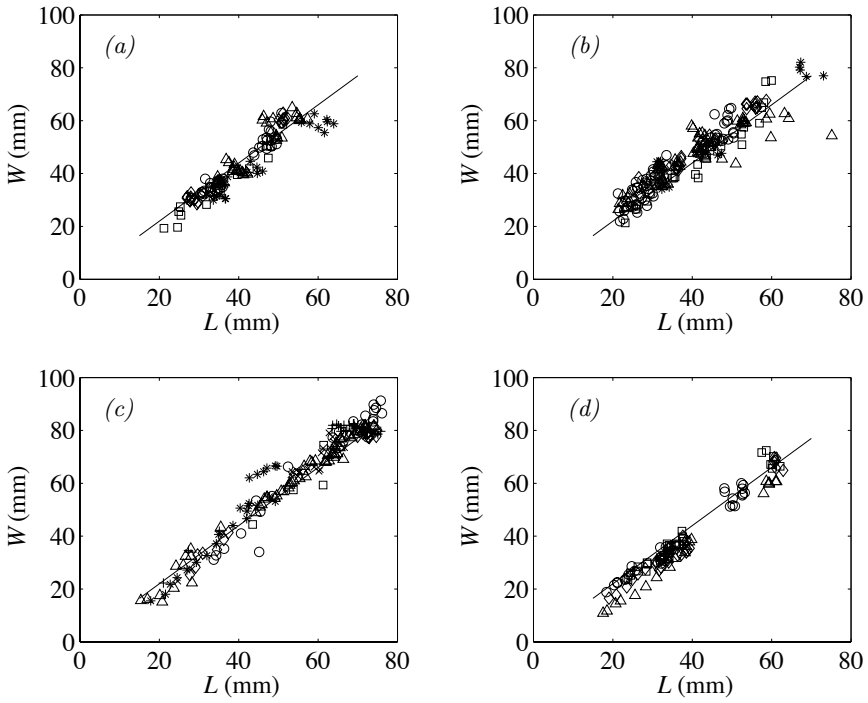

FIGURE 9. Width W versus length L for all dunes, for Reynolds number $Re = 13900$ ($*$), $Re = 16200$ ($\triangle$), $Re = 17400$ ($+$), $Re = 18500$ ($\diamond$), $Re = 19700$ ($\times$), $Re = 20800$ ($\circ$), $Re = 23100$ ($\square$). (a), series 1; (b), series 2; (c), series 3; (d), series 4; the straight line corresponds to eq. (3.4).

at the brink (*i.e.* that the summit of the fitting curve is located downstream of the brink, at a distance of the order of the dune height) was quite general in the explored range of fluid flow rates.

The characteristic lengths defined in Figure 1c have been measured for a large number of dunes, more than six hundreds, as they had reached their equilibrium shape, i.e. after they had travelled a distance larger than twice the size of the initial heap. Figure 9a displays the width W versus the length L for Series 1, for seven flow Reynolds numbers. It appears the data points gather close to the straight line

$$W = c_W\, L, \qquad \text{with} \quad c_W = 1.1, \tag{3.4}$$

with no significant dependence on the flow Reynolds number Re. The scatter, although not negligible, is however much smaller than that for desert dunes, because of the constant direction and velocity of the water flow. Comparison of Figures 9a-c (glass particles of the same density) shows that increasing the grain diameter by a factor 5 has no significant effect on the relationship between L and W. Comparing Figures 9b and 9d (particles with the same diameter and density increased by a factor 1.5), no significant change can again be noted. Finally, the linear relationship between the width and length appears to be independent of the particle diameter and density, as well as of the flow velocity, and (3.4) provides a good fit for all the measurements.

Dune heights were measured with the help of the video camera and the inclined mirror. These heights exhibited large scatter for both physical reasons (loose selection mechanism

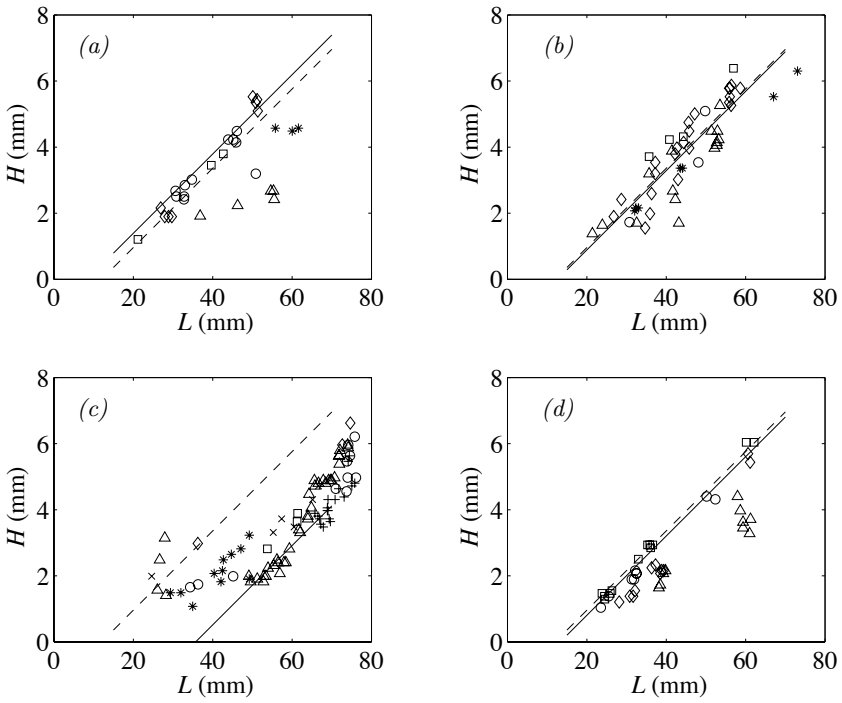

FIGURE 10. Height H versus length L, for same Reynolds numbers as in Figure 9 (same symbols). (a), series 1; (b), series 2; (c), series 3; (d), series 4; solid line: (3.5) with $L_0 = 70\,d$; dashed line (3.5) with $L_0 = 12\,\mathrm{mm}$.

of the height for given horizontal size) and technical reasons (uncertainties related to the use of the mirror system). However, it appeared that the scatter could be reduced by removing the most asymmetric dunes, i.e. dunes with horns of quite different lengths as that shown in Figure 7. Figure 10 displays the height of dunes whose horn lenghts differ by less than 20% of their mean value (this corresponds to the removal of 60% of the measurements). For Series 1 (Figure 10a), most data points gather close to the solid line defined as

$$H = c_H(L - L_0) \tag{3.5}$$

with $c_H = 0.12$ and $L_0 = 70\,d$. However, a few dunes have height smaller by a factor 2. Figures 10b and 10d show that doubling the grain diameter or density, the relationship (3.5) still holds; however, a constant offset length $L_0 = 12\,\mathrm{mm}$ (dashed line) also provides a good fit of the data from the three series 1, 2 and 4. The dune heights from series 3 (large glass grains, Figure 10c) exhibit more complicated features: large dunes ($L \gtrsim 50$ mm) are still accounted for by the relation (3.5) with $L_0 = 70\,d$, but small dunes are closer to the line with $L_0 = 12\,\mathrm{mm}$; the departure from (3.5) may be due to the small ratio H/d of these dunes.

Horns are the most distinctive feature of barchan dunes and play an essential role in their stability (Hersen 2004), so that horn lengths may be considered as their most relevant geometrical property. Figure 11 displays the horn length L_h versus the length L, for the same symmetric dunes as in Figure 10. Figure 11a for Series 1 shows that the

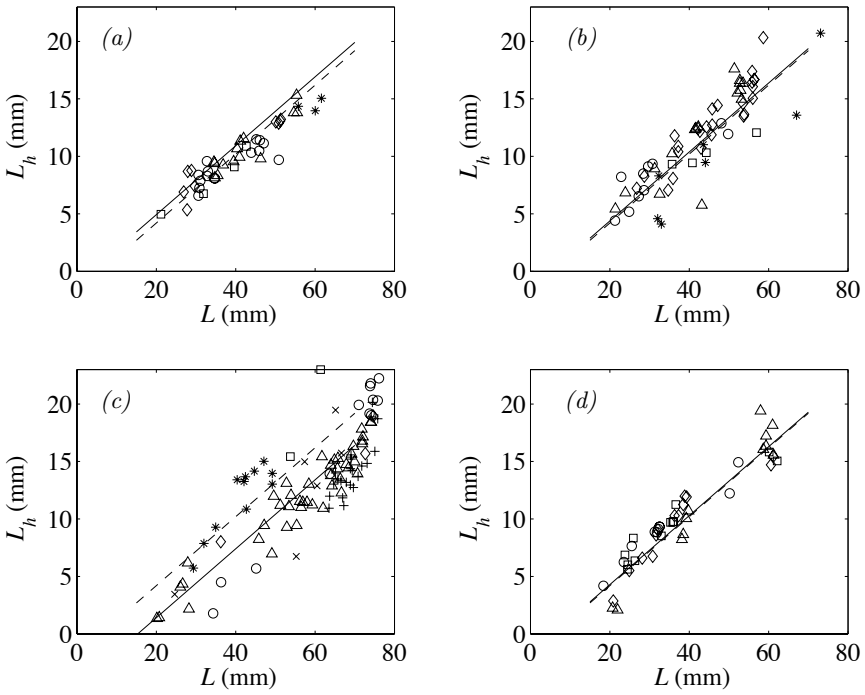

FIGURE 11. Horn length L_h versus length L, for same Reynolds numbers as in Figure 9 (same symbols). (a), series 1; (b), series 2; (c), series 3; (d), series 4; solid line: (3.6) with $L_{0h} = 30\,d$; dashed line (3.6) with $L_{0h} = 6\,\mathrm{mm}$.

horn length L_h increases linearly with the length L, according to the relationship

$$L_h = c_h(L - L_{0h}), \tag{3.6}$$

with $c_h = 0.3$ and $L_{0h} = 30\,d$. Again, no dependence on the flow Reynolds number is visible. Doubling the grain diameter (Figure 11b for series 2) or the relative density (Figure 11d for series 4) does not change the relationship (3.6); however, a constant offset length $L_{0h} = 6\,\mathrm{mm}$ would also provide a good fit (see the dashed lines), as for the dune heights. The dunes from series 3 shown in Figure 11c have shorter horns, still distributed close to (3.6) although the scatter is large; this scatter is likely to be related, again, to small heights ($H/d < 10$). From (3.5) and (3.6), the heights and horn lengths appear to be nearly proportional, as noted by Andreotti *et al.* (2002a) for aeolian dunes.

Finally, the relationships between the dimensions of barchan dunes in water appear to be linear, similarly to those for aeolian dunes. No significant change appears in the slope coefficients c_W, c_H and c_h, by varying the diameter by a factor 2 (between Series 1 and 2), or the density by a factor 1.5 (between Series 2 and 4), or the flow velocity by a factor 1.7 (for all Series). The offset lengths L_0 and L_{0h} do not depend on the particle density and the flow velocity; they might depend on the particle diameter but a specific investigation of small dunes would however be needed for a definite conclusion to be drawn.

The above linear relations between the dune dimensions are similar to those found by previous investigations, with similar slope coefficients c_W, c_H and c_h. In particular, Hersen *et al.* (2002) and Hersen (2005) found $c_H = 0.11$ for subaqueous dunes (we

find 0.12); for aeolian dunes, Sauermann *et al.* (2000) found $c_H = 0.16$ in Southern Morocco and the compilation by Andreotti *et al.* (2002a) gives $c_H = 0.18$. The offset length L_0 and L_{0h}, which break the self-similarity of small dunes, are however quite different: whereas they are of a tens of meters for aeolian dunes, they are much smaller, of about ten millimeters, for subaqueous dunes. As noted by Hersen *et al.* (2002), using $\ell_{\rm drag} = (\rho_p/\rho)d$ as the length scale for the dune dimensions, the data for subaqueaous and aeolian dunes nearly gather. This point will be discussed further in §3.6.

3.4. *Dune velocity*

Let's first consider the classical theory for the velocity $V_{\rm d}$ of a two-dimensional aeolian dune (invariant in the transverse direction) with brink normal to the air flow, without any sand flux from upstream (Bagnold 1941). As long as the volumetric grain flux per unit width at the brink, q_H, is deposited on the avalanche face, mass conservation gives the velocity

$$V_{\rm d} = \frac{q_H}{H}, \tag{3.7}$$

where H is the height of the brink. This equation can also be derived from the local mass conservation equation $\partial_t h + \partial_x q = 0$ with the shape-invariance condition $\partial_t h = -V_{\rm d}\partial_x h$. Integrating this equation along the windward face gives

$$q_H - q(x) = V_{\rm d}(H - h(x)),$$

which relates the local particle flux $q(x)$ to the local dune height $h(x)$. From this equation, (3.7) is recovered when the incoming flux from upstream is zero ($q = 0$ at the foot of the dune where $h = 0$). Assuming that the particle flux q_H is in equilibrium with the local shear stress τ_H at the brink, which is approximately 1.8 times the shear stress $\rho_{\rm air}u_*^2$ over the surrounding flat ground (Andreotti *et al.* 2002a), a semi-empirical transport law of the form $q_H \propto (\rho_{\rm air}/\rho_p)u_*^3/g$ can then be used. From these considerations, the dune velocity is given by

$$\frac{V_{\rm d}}{u_*} \propto \frac{\rho_{\rm air}}{\rho_p}\,\frac{u_*^2}{gH}.$$

This crude model gives the right order of magnitude of a few tens of meters per year. However, the available observations clearly show that the scaling $V_{\rm d} \propto 1/H$ overestimates the velocity of small dunes. Improvements have been proposed, accounting for a better description of the hydrodynamics over the dune and the retarding effect of particle inertia on the particle flux (Andreotti *et al.* 2002b; Kroy *et al.* 2002; Hersen 2004). In particular, relationships of the form $V_{\rm d} \propto 1/(H + H_0)$, where H_0 is an offset height of a few meters, or $V_{\rm d} \propto 1/L$, were shown to provide better predictions. Thorough assessment of these theories however comes up against the difficulty of observations on large space and time scales, and also the large scatter due to the variable flow conditions and sand supply in the open atmosphere.

Under water, a straightforward translation of the theory sketched above consists in replacing the transport law $q_H \propto (\rho_{\rm air}/\rho_p)u_*^3/g$ by one for water, *e.g.* the widely used Meyer-Peter & Müller law (Wong & Parker 2006),

$$\frac{q_H}{V_{\rm ref}d} = 4.0\,(\theta_H - \theta_t)^{3/2}, \tag{3.8}$$

where θ_H is the Shields number (2.5) with the shear stress evaluated at the brink, and $V_{\rm ref} = ((\rho_p/\rho - 1)gd)^{1/2}$. (Note that in the limit of small fluid density and large shear stress, (3.8) reduces to the relationship for air.) To our knowledge, the only observations of the velocity of subaqueous dunes are those of Hersen (2005) for dunes on a tray

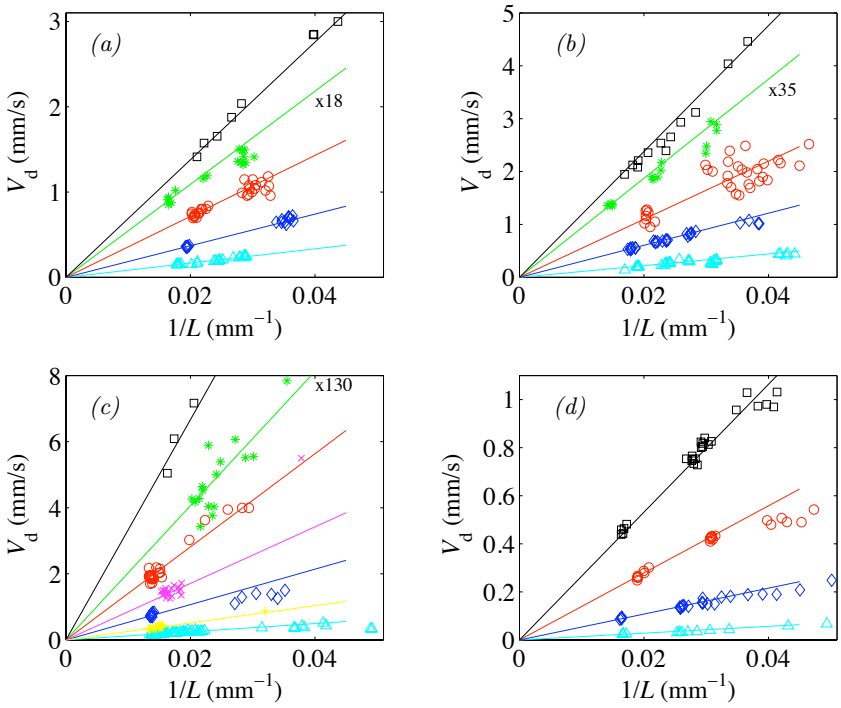

FIGURE 12. Dune velocity V_d versus the inverse length $1/L$ for series 1 (a), series 2 (b), series 3 (c) and series 4 (d). Symbols correspond to given Reynolds number, see caption of Figure 9 (for the lowest one ($*$), the small velocity is multiplied by the factor shown on the right of the line). Straight lines emphasize the linear dependence $V_d \propto 1/L$ for given flow conditions.

undergoing asymmetric oscillations, and of Taniguchi & Endo (2007) for dunes under alternating flows. Thus, no velocity measurement under steady conditions is available, so that the prediction (3.7-3.8) has not been assessed yet.

In the present experiments, dune velocities have been investigated by varying both the grain properties and the fluid velocity. Velocities have been determined from the distance travelled by the foot of the slip face, divided by the corresponding time; the distance was of a few dune lengths (typically between 10 or 20 centimeters), and times ranged from 20 seconds to 40 minutes.

Figure 12 displays the velocity V_d as a function of the inverse dune length L^{-1}, for several flow Reynolds number, and for the four series (for clarity, the small values of V_d for the smallest Reynolds number ($*$) have been multiplied by the coefficient shown on the right of the line). For the small glass particles of series 1, Figure 12a shows that, for given Reynolds number, the velocity scales with the inverse length, $V_d \propto L^{-1}$, as predicted by the mass conservation argument (3.7) along with the scale invariance $L \propto H$. Figures 12b-c-d display the dune velocity for the series 2, 3 and 4, showing the same features. For the smallest Reynolds number, linear regression suggested that the velocity rather follows $V_d \propto (L + L_0)^{-1}$, with a length L_0 of a few millimeters, but the scatter of the measurements prevented any precise determination.

The increase of the dune velocity with Reynolds number, for given dune length, is also clearly visible in Figure 12. This dependence has been studied further by considering the velocity $V_{d,60}$ of dunes of the same length, $L = 60$ mm, obtained from the linear

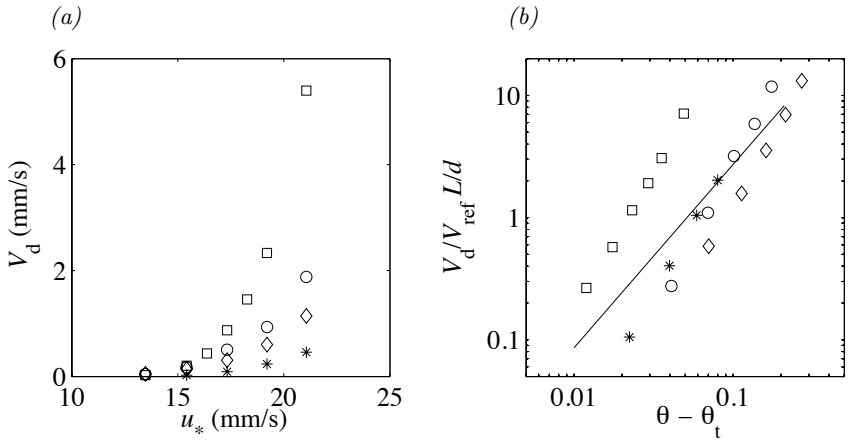

FIGURE 13. Velocity of dunes with the same length $L = 60$ mm, for all series (see Table 1 for symbols); (a), dimensional velocity versus the wall friction velocity u_*; (b), normalized velocity $V_\mathrm{d}/V_\mathrm{ref}(L/d)$ versus $\theta - \theta_t$ in log-log scales; straight line: eq. (3.7).

regression lines; such dunes all have nearly the same height, about 5–6 mm according to (3.5). As shown in Figure 13a for all series, the velocity $V_{\mathrm{d},60}$ increases strongly with the friction velocity u_*; for given u_*, it increases with the particle diameter (compare series 1, 2 and 3 for the glass particles), and decreases with the particle density (compare series 2 and 4 for the glass and zirconium particles of nearly same diameter $d \approx 0.2$ mm). For each of the four series, extrapolating the velocity down to zero provides an estimate of the threshold friction velocity below which the dune no longer moves. This threshold is in good agreement with that found independently from the visual observation of the stopping of particle motion at the dune surface, and reported in Table 2.

In order to assess Bagnold's theory, Figure 13b displays the dune velocity, normalized with $V_\mathrm{ref}d/L$, as a function of $\theta - \theta_t$, in logarithmic scales. Shields numbers have been calculated with the friction velocity $u_{*d} = 1.2\,u_*$, i.e. by assuming that the ratio 1.2 found at threshold still holds above threshold. It appears that for all the four series, the dune velocity follows power laws of the form $V_\mathrm{d}/V_\mathrm{ref} \propto (d/L)(\theta - \theta_t)^n$, with the same exponent $n \approx 2.5$ but different numerical coefficients. Figure 13b also displays the line corresponding to Bagnold's prediction (3.7) with the particle flux at the crest given by the Meyer-Peter & Müller correlation. It appears clearly that this prediction does not provide the right velocity:

- it does not account for the dependence on the type of particles;
- the exponent 3/2 of the power law is too small.

Note that taking a different bedload transport law, from those available in the litterature, do not provide better agreement.

Attempting to gather the data points of the four series on the same master curve, it first appeared that dividing the dune velocity by the true falling velocity V_fall or the friction velocity u_{*d}, instead of the reference velocity V_ref, does not improve significantly the picture. In fact, Figure 13b strongly suggests that one single dimensionless parameter, i.e. the Shields number, is not sufficient to account for dune velocities. This observation is consistent with the fact that particle Reynolds numbers are not large (see Table 1), so that some dependence with this number may be expected.

A good collapse of the data points is achieved when the dune velocity is divided

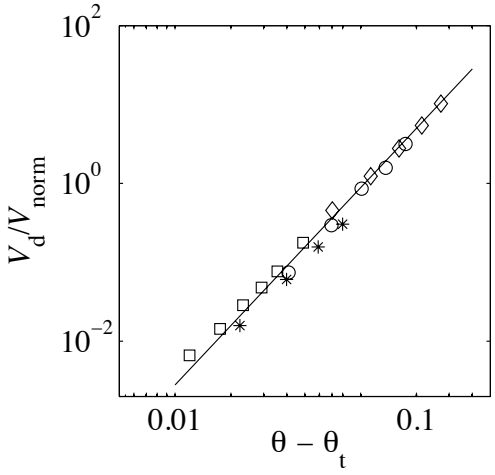

FIGURE 14. Normalized dune velocity versus $\theta - \theta_t$ in log-log scales, for all series (see Table 1 for symbols). $V_{\rm norm} = V_{\rm ref} Re_s d/L$, straight line: eq. (3.9).

by the sedimentation Reynolds number, as shown in Figure 14 where the straight line corresponds to

$$\frac{V_{\rm d}}{V_{\rm ref}} = 280\, Re_s\, \frac{d}{L}(\theta - \theta_t)^{2.5}. \tag{3.9}$$

From (3.9), the particle flux q_H at the dune crest can be deduced from the mass conservation equation (3.7) and the morphological relation (3.5). Ignoring the small offset length L_0 in (3.5), q_H is found to be

$$\frac{q_H}{V_{\rm ref} d} = 34\, Re_s (\theta - \theta_t)^{2.5}. \tag{3.10}$$

This relation is different, as expected, from the usual relationships for turbulent flow which typically involve the exponent 3/2 for the dependence with the Shields number, as the Peter-Meyer & Müller relation (3.8). It is also different, although closer, from the quadratic relation $q_H/V_{\rm ref} d \propto \theta(\theta - \theta_t)$ found from viscous flow experiments on a flat bed by Charru, Mouilleron & Eiff (2004) (in these experiments, the grain properties were not varied so that Re_s was constant). Note that the closeness of (3.10) with viscous flow results is consistent with the fact that here, the particle Reynolds number was always smaller than 13 (see Table 1), so that the moving grains hardly emerged from the viscous sublayer (this point will be discussed further in the Part 2 of this paper, in relation with shear stress measurements). Finally, (3.9) appears as as a good fit for grains with different density and diameter, but its physical meaning remains to be understood.

3.5. *Erosion rate*

As a dune propagates, it slowly looses particles at the horn tips and its size decreases. Understanding this particle leakage is important in the perspective of modelling the evolution of a field of dunes, where the particles leaving one dune feed another one downstream.

In the present experiments, a few single dunes have been tracked during a sufficiently long time for their size evolution to be measured until disappearance. Figure 15a displays the time evolution of the width of four dunes, for two types of particles (series 3 and 4) and

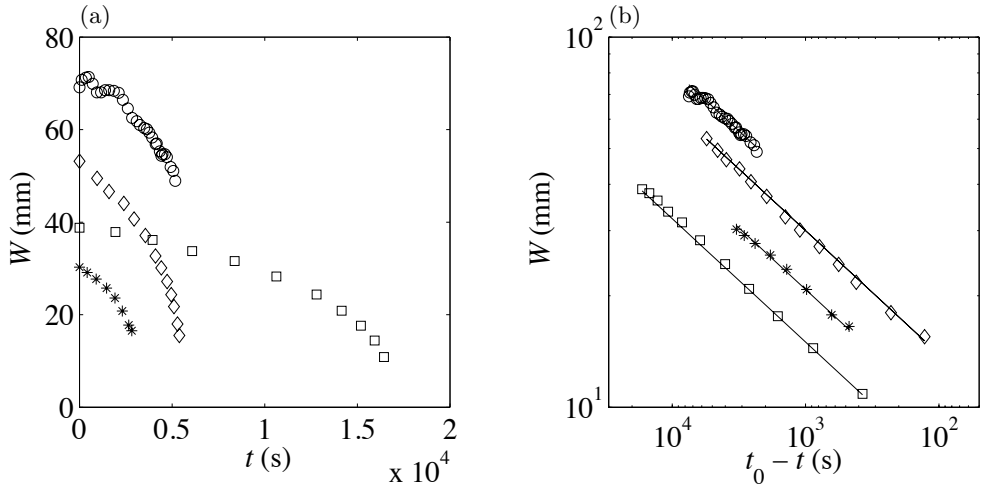

FIGURE 15. Time variation of the dune width: (a), linear scales; (b), log scales. Symbols: ($\diamond$): series 3, $Re = 13900$; ($\circ$): series 3, $Re = 16200$; ($\square$): series 4, $Re = 16200$; ($*$): series 4, $Re = 18500$; (—): power law (3.11).

three Reynolds numbers. As the dune size has decreased down to about one centimeter, the horns become unstable, randomly disappearing and appearing again with a time scale of a few seconds. After a few oscillations, the horns definitely disappear and the remaining heap is dispersed by the fluctuations of the turbulent flow. The disappearance occcurs at a critical time t_0 after the beginning of the run, which was typically between one and five hours (larger dunes had longer life times). From the measurement of the critical time or its estimation when the tracking was stopped before the disappearance of the dune, the width was found to follow the power law $W \propto (t_0 - t)^{1/3}$, as shown by the log-log plot in Figure 15b.

From the morphology study presented in section 3.3 and on considering that dunes have self-similar parabolic shapes, their volume $\mathcal{V}$ is related to their width by

$$\mathcal{V} \approx \frac{6}{15}\,\frac{c_H}{c_W^2}\,W^3 \approx 0.03\,W^3.$$

Thus the exponent $1/3$ for $W(t)$ corresponds to linear decrease of the volume, i.e. constant number of particles leaving the horns per unit time, or constant erosion rate. (Note that an erosion rate proportional to the volume of the dune would result in an exponential decrease, which is clearly not the case here.) Let t_e be the erosion time, i.e. the time needed for loosing one grain per horn. Then the variation of the volume of the dune during $\mathrm{d}t$ is

$$\mathrm{d}\mathcal{V} = -2\frac{\pi d^3}{6\phi}\,\frac{\mathrm{d}t}{t_e}$$

where $\phi \approx 0.6$ is the volume fraction of the particles. From the above relations, the dune width decreases with time as

$$\frac{W}{d} = 3.9\left(\frac{t_0 - t}{t_e}\right)^{1/3}. \tag{3.11}$$

From the above relation and the measured time evolution $W(t)$, the erosion time t_e can be deduced for each experiment. The four erosion times corresponding to Figure 15

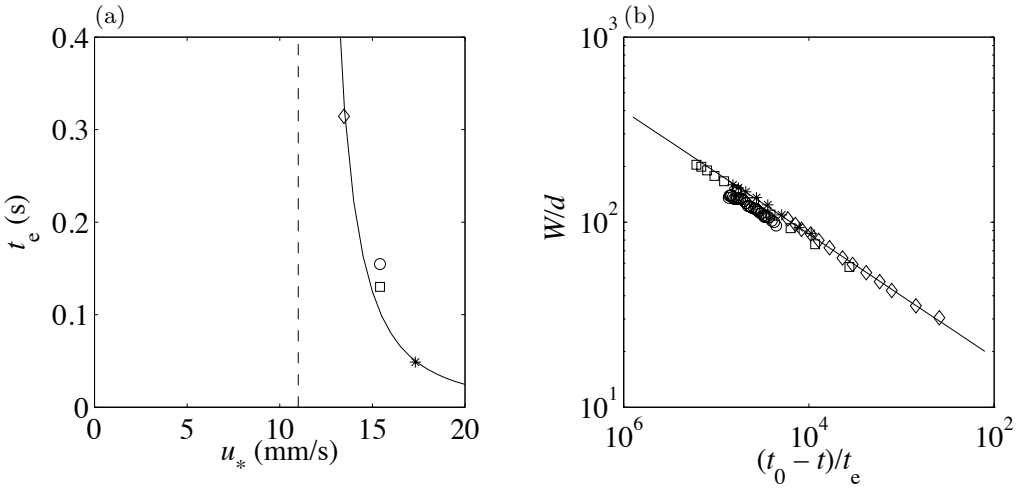

FIGURE 16. (a) Erosion time from experiments (symbols) and correlation (3.12) (solid line); (b), dimensionless width versus dimensionless time using the correlation (3.12) for t_e. ($\diamond$), series 3, $Re = 13900$; ($\circ$), series 3, $Re = 16200$; ($\square$), series 4, $Re = 16200$; ($*$), series 4, $Re = 18500$.

are shown in Figure 16a, where they appear to depend mainly on the shear velocity u_* (they are nearly equal at the same flow Reynolds number $Re = 16200$ for series 3 and 4). Since the particles at the horn tips hardly emerge from the viscous sublayer (small particle Reynolds numbers), the expected scale for the erosion time is the viscous time based on the wall scales u_* and ν. It appeared that the following law fits reasonably well the measured erosion times:

$$t_e = 2\,\frac{\nu}{(u_* - u_{*e})^2}, \qquad u_{*e} = 11\,\mathrm{mm\,s^{-1}} \tag{3.12}$$

where u_{*e} is a threshold friction velocity for dune erosion (the erosion time must diverge at threshold). This threshold appears to be slightly lower than the threshold u_{*t} for dune motion, which can be understood by the fact that particles are easier to move on the smooth wall at the tip of the horns than on the rough dune surface. Figure 16b shows that with the above modelling for the erosion time, all the data points collapse reasonably well on the same curve for the four dunes.

3.6. *Minimum size*

As noted by Bagnold (1941, §14.3), aeolian barchan dunes have a minimum height of about $H_{\min} \approx 1$ m, and a corresponding minimum length $L_{\min} \approx 10$ m, below which no dune is observed. The minimum height was interpreted by Bagnold by considering the trajectories of the sand grains after they have passed over the brink and enter a region of stagnant air: below some critical dune height, the grains fall beyond the foot of the slip face and are dispersed by the wind. From another point of view, the minimum length can be interpreted as the distance needed for the particle flux to increase from zero, at the upwind foot of the dune, up to some saturated value depending on the local shear stress only (Bagnold 1941, §12.9). The length scale associated with the relaxation of the particle flux may be related to several physical phenomena. Sauermann, Kroy &

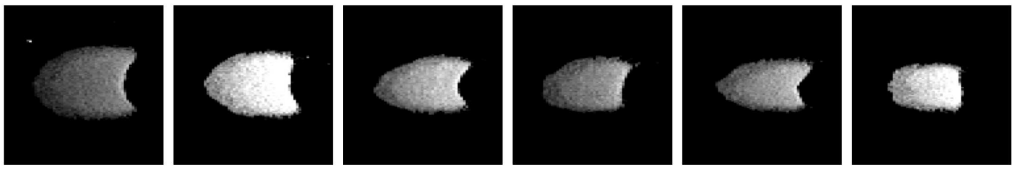

FIGURE 17. Successive pictures of the oscillations of the horns and disappearance of a barchan dune. Between the first and last pictures, the elapsed time is 20 seconds and the dune has travelled a distance of four times its initial size, of 15 mm.

Hermann (2001) proposed that it should scale with the saltation length

$$\ell_{\rm salt} \approx 15\,\frac{u_*^2}{g} \tag{3.13}$$

of the grains expelled from the bed by the impact of the oncoming grains, with a prefactor accounting for the slowing down of the wind by the saltating cloud. Andreotti *et al.* (2002b) consider that grain inertia is the dominant mechanism involved in the saturation, so that the relevant length should be an acceleration length of the particles accelerated from rest by the wind. From dimensional analysis, this acceleration length must scale with the drag length

$$\ell_{\rm drag} = \frac{\rho_p}{\rho}\,d \tag{3.14}$$

(which is typically 0.5 meter), and weakly depends on the wind strength (Andreotti *et al.* 2010). These ideas have also been applied to observations on Mars by Claudin & Andreotti (2006).

Under water, whose density is one thousand times larger than that of air, hydrodynamic interactions are more complex, and particles roll on each other rather than experience large saltating jumps (Lajeunesse *et al.* 2010). A characteristic length may however dominate: the deposition length

$$\ell_{\rm fall} = \frac{u_*}{V_{\rm fall}} d, \tag{3.15}$$

which represents the distance travelled by a grain with velocity u_* during the falling time $d/V_{\rm fall}$. This length was introduced by Charru and Hinch (2006) from an erosion-deposition model, and its importance in the selection of the wavelength of ripples was discussed by Charru (2006). In water, the lengths $\ell_{\rm drag}$ and $\ell_{\rm fall}$ are of the order of one millimeter, but they scale differently with the parameters. The measurements reported in this section are intended to discuss the existence of a minimum size of subaqueous barchan dunes, and to assess the relevance of $\ell_{\rm drag}$ or $\ell_{\rm fall}$ as the scaling length for this minimum size.

Turning back to our experiments, the size of a dune was found to decrease slowly in the course of its motion, because of the small leakage of particles at the tip of the horns as discussed in the previous section. As the size is reduced to the order of one centimeter, the horns become unstable, disappearing and reappearing randomly, as shown by the sequence of six successive photographs displayed in Figure 17. The leakage of particles increases strongly, and after a few oscillations of the horns (a few seconds) the dune disappears.

The time of the disappearance, and the corresponding dune size, were not easy to define precisely, but the onset of the horn instability was found to be reproducible. The

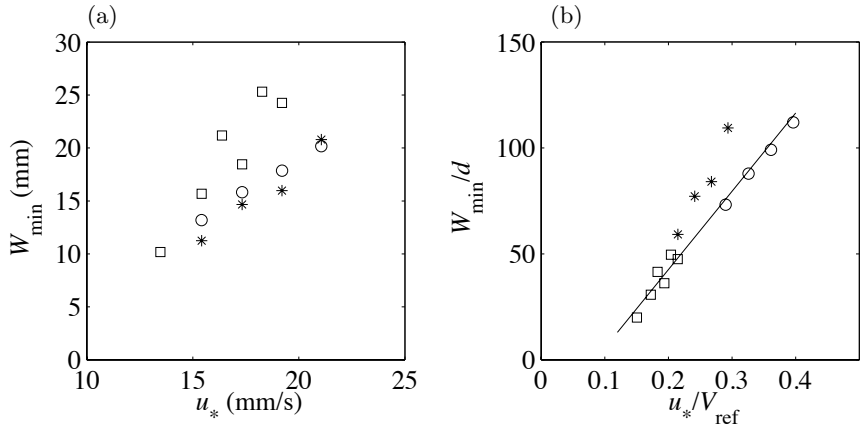

FIGURE 18. (a) Minimum width of barchan dunes as a function of the shear velocity, for dunes from series 2 (∘), 3 (□) and 4 (∗). (b) Same data presented with d and V_{ref} as the unit length and unit velocity.

size of a barchan dune at the onset of the instability was defined as the minimum size. Figure 18a displays the variation of the minimum dune width, $W_{\min}$, with the friction velocity u_*, for the three series 2, 3 and 4. For a given series, $W_{\min}$ appears to increase linearly with u_*. Were the drag length (3.14) be the relevant scaling length, $W_{\min}$ should not depend on u_*, which is clearly not the case. Figure 18b displays the same data in dimensionless form, using d and V_{ref} as the length and velocity units. The data points for the glass beads of diameter 0.2 and 0.5 mm (series 2 and 4) fall on the same line, and those for the zirconium beads (series 3) fall slightly above. Thus, although the data points for the heavy zirconium grains lie slightly above the others, the deposition length $(u_*/V_{\mathrm{ref}})d$ appears to be a scaling length of the minimum width (note that using the actual falling velocity V_{fall} instead of V_{ref} provides a less good collapse). Finally, the result that the minimum width scales with a deposition length is consistent with both ideas presented at the beginning of this section: dunes disappear because they become smaller than the saturation length of the grain flux over the dune, or because the grains leaving the brink (with velocity of the order of u_*) fall beyond the foot of the slip face and disperse in the wake.

3.7. *Stripes of particles*

Illuminating dunes with an almost horizontal light revealed, on their upstream face, streamwise stripes with regular spacing, as shown in Figure 19. These stripes were unsteady, moving laterally back and forth, with a lifetime of a few seconds. They were observed for all Reynolds numbers in the explored range and with the four series of particles. These stripes were identified as the trace of fluid "streaks", the filaments of streamwise low-speed fluid which spread in the inner layer of turbulent boundary layers (Smith & Metzler 1983, Panton 2001, Davidson 2004). Streaks are known to develop in the viscous sublayer ($y^+ < 5$) with a well-defined spacing or spanwise wavelength, λ, scaling with the viscous length ν/u_* such that $\lambda^+ \approx 75 - 80$. Then they are lifted in the logarithmic region where their spacing increases as the result of merging or coalescence. Streaks are no longer visible above $y^+ = 40$. In the present experiments, the domain of existence of the streaks, $y^+ < 40$, typically corresponds to 2 to 4 mm, which is the order of magnitude of the dune heights. The alternance of regions of higher and lower

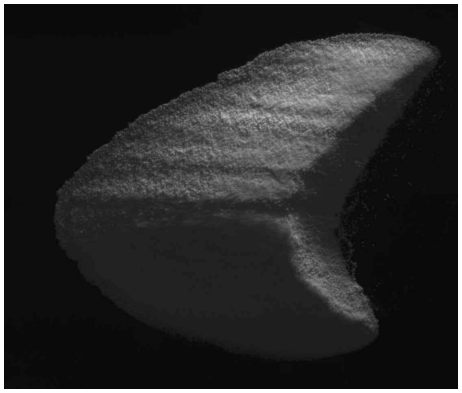

FIGURE 19. Top view of a dune illuminated with an almost horizontal light, showing streamwise stripes (the flow is from left to right, particles from series 4).

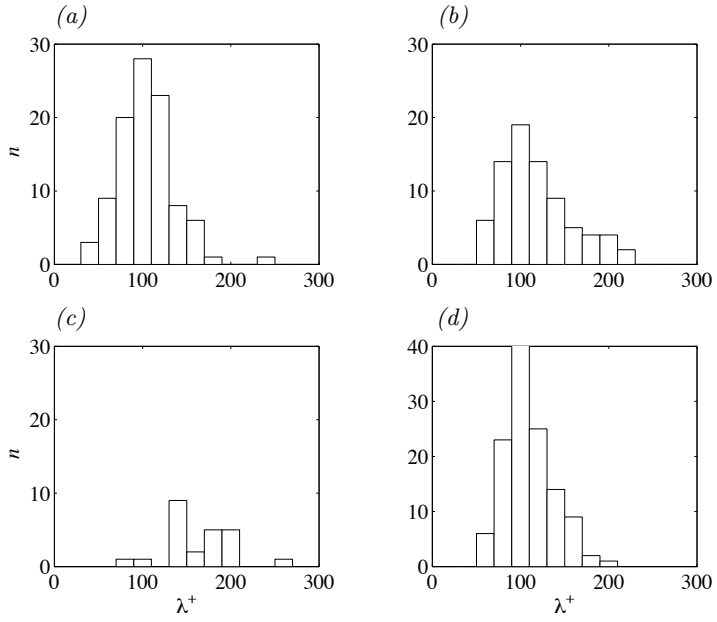

FIGURE 20. Histograms of the dimensionless spanwise spacing of the stripes $\lambda^+ = \lambda u_*/\nu$, for (a) series 1, (b) series 2, (c) series 3, (d) series 4.

velocity is associated with pairs of counter-rotating streamwise vortices, which promote higher erosion of particles along the lines where the streamwise velocity is higher and the spanwise velocity diverges, and higher deposition in between these lines, explaining the observed relief.

The spacing λ of particle stripes was measured for flow Reynolds numbers in the range 18000–28000, for the four series of particles. Figure 20 displays the distribution of these

wavelengths, in wall units. It appears that for the particles of series 1, 2 and 4 (Figures 20a, 20b and 20d), with diameter in the range 0.1–0.2 mm corresponding to $d^+ = 1.7$–4.5, the distribution has a well-defined peak at $\lambda^+ \approx 100$, and a long tail on the side of large wavelengths. For the larger particles of series 3 ($d = 0.5$ mm, $d^+ = 9.7$–13.3, Figure 20c), which protude out of the viscous sublayer, the distribution, although not converged, indicates a larger spacing of about $\lambda^+ \approx 150$. These values correspond to those of streaks on smooth walls (Smith & Metzler 1983), and confirm that the observed stripes of particles are traces of fluid streaks.

Another mechanism could be invoked for the existence of stripes, related to the curvature of the streamlines over a dune: the centrifugal Görtler instability of a boundary layer flow over a concave wall. For a turbulent boundary layer, this instability gives rise to unsteady streamwise vortices, and has been recognized to be responsible of sand stripes in the scour-hole problem of a wall-jet flowing over a bed of particles (Hopfinger *et al.* 2004). However, as shown below, this instability is not relevant here. For the appearance of Görtler vortices, the curvature R^{-1} must be high enough; the condition usually considered, $\delta/R \geq 0.01$ (Floryan 1991), with $R = H/L^2$, is fulfilled here. However, the instability is weak and the growth of the vortices noticeably slow; following Hopfinger *et al.* (2004), the spatial growth rate is $(Re_{\delta_m}\delta_m)^{-1}$, where δ_m is the momentum thickness and Re_{δ_m} is a Reynolds number based on δ_m and an eddy viscosity such that $Re_{\delta_m} \approx 30$. With $\delta_m \approx \delta/10$, the typical distance from the upstream foot of a dune at which the instability might be observed would be $3\delta = 90$ mm, which is larger than all the observed dune lengths. Moreover, the centrifugal instability amplifies the largest eddies present in the boundary layer, leading to vortices with spanwise wavelength usually about twice the boundary layer thickness (Floryan 1991). Such a wavelength, here of 60 mm, is much larger than the observed ones. Therefore, the Görtler instability cannot be invoked for explaining the observed stripes. Finally, it can be noted that streaks may represent an important mobilizing force in the erosion process, corresponding to an effective shear stress, active in the sediment transport, larger than the actual shear stress.

4. Summary and conclusion

When a liquid flow transports a small amount of heavy particles, the particles gather to form dunes with crescentic shape, with size of a few centimeters. Their main features are a gentle slope on the upstream face, a sharp brink above a slip face downstream, and horns pointing downstream. These dunes, similar to the barchan dunes observed in deserts, are very robust structures. Their turnover time, i.e. the time needed for a dune to travel a distance equal to its length, is of the order of one minute, which makes subaqueous dunes much easier to study than the much larger and slower aeolian dunes (for which the turnover time is of the order of one year). The geometrical and dynamical properties of several hundreds of these dunes were investigated for flow Reynolds number up to 21000, for four types of grains of different diameter and density. The main observations can be summarized as follows.

- A heap of particles deposited in the channel quickly evolves to a barchan dune, within a time of the order of their turnover time.
- The width, height and horns length are linear functions of the dune length, with an offset of a few millimeters which breaks the self-similarity of small dunes. These relations appear to be independent of the fluid velocity and the grain density and diameter. The offset length may however depend weakly on the particle diameter, but the scatter of the measurements prevented any definite conclusion to be drawn about this point. The slope

of the upstream dune profile does not vanish at the brink: the summit of the envelope of the profile is situated at a distance of about one dune height downstream.

• For small flow rates, the particles are at rest and the dune does not move. From the Shields curve and visual observation of the onset of particle motion, it was found that the shear stress on the dune, ρu_{*d}^2, is larger by a factor 1.4 than that on the smooth wall of the channel.

• The velocity of dunes was found to be inversely proportional to their size, as predicted by a mass conservation argument. An empirical relationship for the dimensionless velocity was derived, on which all the data points collapse well. This relationship involves not only on the dimensionless shear stress (the Shields number θ) but also sedimentation Reynolds number (or the particle Reynolds number). This suggests that viscous effects are not negligible with regard to the particle transport, which is consistent with the fact the particle diameter, in wall units ν/u_{*d}, was smaller than 13.

• As a dune migrates, it looses a few particles at the tip of its horns, so that its size slowly decreases. The width was found to decrease according to the power law $(W/d)^3 \propto (t_0 - t)/t_e$ where t_0 corresponds to the dune disappearance and t_e is an erosion time. A consequence of this law is that erosion does not depend on the dune size and is governed by the hydrodynamics in the vicinity of the horn tip. Modelling the erosion time with a viscous scale, all the traces of $W(t)$ collapse on the same curve.

• Barchan dunes exhibit a minimum size below which the horns become unstable and oscillate and the dune quickly disappears. The minimum width increases linearly with the friction velocity and scales roughly with the deposition length $\sqrt{\theta}\, d$. This result is consistent with two different explanations: dunes disappear because they become smaller than the saturation length of the grain flux over the dune, or because the grains leaving the brink fall beyond the foot of the slip face and disperse in the wake.

• Longitudinal stripes of particles were observed on the upstream face of the dunes. These stripes have a spanwise spacing $\lambda^+ \approx 150$, in wall units, and are formed by the well-known longitudinal streaks which develop in the viscous sublayer of a turbulent boundary layer. These streaks are likely to enhance particle transport.

Finally, subaqueous barchan dunes appear as very robust structures which may migrate over long distances. At moderate flow rates, they are the main mode of particle transport. Their outstanding stability properties —which are likely to involve the small spanwise particle flux, particle relaxation effects, and the flow structure in the dune wake— remain to be understood. Beyond the study of isolated dunes, two situations would also be of interest: (i) as the particle flux is increased, dunes with different size and different velocity interact, and may form a continuous rippled bed; (ii) as the fluid flow rate is increased, particles escape the dune brink and suspension occurs. These questions are left for future investigation.

We are grateful to the French Agence Nationale de la Recherche for partial financial support of this study (#ANR-07-BLAN-0180-01), and to the Brazilian government foundation CAPES for the scholarship grant of E. M. Franklin.

REFERENCES

Al-lababidi, S., Yan, W., Yeung, H., Sugarman, P. & Fairhurst, C. P. 2008 Sand transport characteristics in water and two-phase air/water flows in pipelines. *Proc. of the 6th North American Conference on Multiphase Technology*, 159–174.

Andreotti, B., Claudin, P. & Douady, S. 2002a Selection of dune shapes and velocities. Part 1: dynamics of sand, wind and barchans. *Eur. Phys. J. B* **28**, 321–339.

Andreotti, B., Claudin, P. & Douady, S. 2002b Selection of dune shapes and velocities. Part 2: a two-dimensional modelling. *Eur. Phys. J. B* **28**, 341–352.

Andreotti, B., Claudin, P. & Pouliquen, O. 2010 Measurements of the aeolian sand transport saturation length. *Geomorphology* **123**, 343–348.

ASCE task committee on flow and transport over dunes 2002 Flow and transport over dunes. *J. Hydr. Engrg.* **128**, 726–728.

Bagnold, R. A. 1941 *The physics of blown sand and desert dunes.* Chapman & Hall, London.

Charru, F. 2006 Selection of the ripple length on a granular bed sheared by a liquid flow. *Phys. Fluids* **18**, 121508.

Charru, F., Mouilleron, H. & Eiff, O. 2004 Erosion and deposition of particles on a bed sheared by a viscous flow. *J. Fluid Mech.* **519**, 55–80.

Claudin, P. & Andreotti, B. 2006 A scaling law for aeolian dunes on Mars, Venus, Earth, and for subaqueous ripples. *Earth Planetary Sci. Lett.* **252**, 30–44.

Clift, R., Grace, J. R. & Weber, M. E. 1978 Bubbles, drops and particles. Academic Press.

Davidson, P. A. 2004 *Turbulence: An Introduction for Scientists and Engineers.* Oxford University Press.

Elbelrhiti, H., Andreotti, B. & Claudin, P. 2008 Barchan dune corridors: field characterization and investigation of control parameters. *J. Geophys. Res.* **113**, F02S15.

Floryan, J. M. 1991 On the Görtler instability of boundary layers. *Prog. Aerospace Sci.* **28**, 235–271.

Hersen, P. 2004 On the crescentic shape of barchan dunes. *Eur. Phys. J. B* **37**, 507—514.

Hersen, P. 2005 Flow effects on the morphology and dynamics of aeolian and subaqueous barchan dunes. *J. Geophys. Res.* **110**, F04S07.

Hersen, P., Douady, S. & Andreotti, B. 2002 Relevant lengthscale of barchan dunes. *Phys. Rev. Lett.* **89**, 264301.

Hopfinger, E. J., Kurniawan, A., Graf, W. H. & Lemmin, U. 2004 Sediment erosion by Görtler vortices: the scour-hole problem. *J. Fluid Mech.* **520**, 327–342.

Hunt, J. C. R., Leibovich, S. & Richards, K. J. 1988 Turbulent shear flows over low hills. *Q. J. R. Meteorol. Soc.* **114**, 1435–1470.

Kroy, K., Sauermann, G. & Herrmann, H. J. 2002 Minimal model for aeolian sand dunes. *Phys. Rev. E* **66**, 031302.

Lajeunesse, E., Malverti, L. & Charru, F. 2010 Bedload transport in turbulent flow at the grain scale: experiments and modeling. *J. Geophys. Res.* **115**, F04001.

Mantz, P. A. 1978 Bedforms produced by fine, cohesionless, granular and flakey sediments under subcritical water flows. *Sedimentology* **25**, 83–103.

Melling, A. & Whitelaw, J. H. 1976 Turbulent flow in a rectangular duct. *J. Fluid Mech.* **78**, 289–315.

Mouilleron, H., Charru, F. & Eiff, O. 2009 Inside the moving layer of a sheared granular bed. *J. Fluid Mech.* **628**, 229–239.

Nagib, H. M. & Chauhan, K. A. 2008 Variations of von Kármán coefficient in canonical flows. *Phys. Fluids* **20**, 101518.

Panton, R. L. 2001 Overview of the self-sustaining mechanisms of wall turbulence. *Prog. Aerospace Sci.* **37**, 341–383.

Sauermann, G., Rognon, P., Poliakov, A. & Herrmann, H. J. 2000 The shape of the barchan dunes of Southern Morocco. *Geomorphology* **36**, 47–62.

Sauermann, G., Kroy, K. & Herrmann, H. J. 2001 Continuum saltation model for sand dunes. *Phys. Rev. E* **64**, 031305.

Schlichting, H. 1979 *Boundary-Layer Theory.* McGraw-Hill.

Smith, C. R. & Metzler, S. P. 1983 The characteristics of low-speed streaks in the near-wall region of a turbulent boundary layer. *J. Fluid Mech.* **129**, 27–54.

Soulsby, R. L. & Whitehouse, R. J. S. 1997 Threshold of sediment motion in coastal environments. *Proc. Australasian Coastal Engng and Ports Conf.*, 149–154.

Taniguchi, K. & Endo, N. 2007 Deformed barchans under alternating flows: Flume experiments and comparison with barchan dunes within Proctor Crater, Mars. *Geomorphology* **90**, 91–100.

Wong, M. & Parker, G. 2006 Reanalysis and Correction of Bed-Load Relation of Meyer-Peter and Mller Using Their Own Database. *J. Hydr. Engrg.*, **132**, 1159–1168.